

# Models for MIMO propagation channels: a review

Kai Yu<sup>\*,†</sup> and Björn Ottersten

Department of Signals,  
Sensors and Systems,  
Royal Institute of Technology,  
SE–100 44 Stockholm,  
Sweden

## Summary

This paper reviews recently published results on multiple input multiple output (MIMO) channel modeling. Both narrowband and wideband models are considered. We distinguish between two main approaches to MIMO channel modeling, that is, physically based and nonphysically based modeling. The nonphysical models primarily rely on the statistical characteristics of the MIMO channels obtained from the measured data, while the physical models describe the MIMO channel (or its distribution) *via* some physical parameters. We briefly review different MIMO channel models and discuss their relationships. Some interesting aspects will be described in more detail and we note areas in which few results are available. Copyright © 2002 John Wiley & Sons, Ltd.

---

## KEY WORDS

wireless communications  
antenna array  
MIMO systems  
MIMO channel capacity  
MIMO channel modeling  
MIMO channel measurements

---

## 1. Introduction

The increasing demand for high data rates and the limited available bandwidth motivates the investigation of wireless systems that efficiently exploit the spatial domain. Because of cost, size, and complexity limitations at the terminal, antenna arrays are usually considered only at the base stations (access points) to

spatially discriminate the desired signal from interference and noise. The use of spatial diversity, both on reception as well as transmission, can improve throughput and coverage in addition to allowing a higher degree of spectral reuse and thereby increase the system capacity.

As recently reported in References [1,2], channel capacity can be greatly increased by using antenna array at both the transmit and the receive side of

\*Correspondence to: Kai Yu, Department of Signals, Sensors and Systems, Royal Institute of Technology, SE–100 44 Stockholm, Sweden.

†E-mail: kaiyu@s3.kth.se

the so-called MIMO systems as long as the environment provides sufficient scattering. Conceptually, an MIMO channel can be seen as a parallel spatial subchannel that allows the transmission of parallel symbol streams. Therefore, the MIMO channel capacity can potentially increase linearly with the number of spatial subchannels (a minimum of the number of receive or transmit antenna elements). This has been demonstrated in Reference [3], in which an architecture (BLAST) was proposed along with a coding and decoding scheme. Some field measurements investigating MIMO channel capacity have recently been reported in References [4–10]. Several of the reported results are encouraging in that the scattering has been sufficiently rich to provide capacities close to the ideal situation.

The propagation conditions determine the channel capacity that can be expected for an MIMO system. It is of great interest to characterize and model the MIMO channel for different conditions in order to predict, simulate, and design high-performance communication systems. Among other advantages, the simulation of MIMO propagation channel can assist in the choice of efficient modulation schemes under different scenarios and system performance can be accurately predicted. Much work has been reported in the single input single output (SISO) channel modeling area. The models for indoor radio channels were reported in References [11–17] while the examples of outdoor channel models can be found in References [18,19]. However, extending these models to the MIMO case is not straightforward. The spatial dimension must now be characterized either directly or indirectly.

In this paper, we review some recently published research on MIMO channel modeling. First, we categorize these models into two main groups, that is, nonphysically and physically based models. The nonphysical models are derived from the statistical characteristics of the MIMO channels, while the physical models use some important physical parameters to provide a reasonable description of the MIMO channel characteristics and the surrounding scattering environment. The MIMO channel models will be reviewed respectively on the basis of the classification in this paper. Some of the MIMO channel models are discussed in detail, while the rest are touched upon briefly. We will also study and discuss the relationships between different MIMO channel models. Measurement results are presented to make comparisons with some proposed models. Finally, we conclude and make a few suggestions for future research.

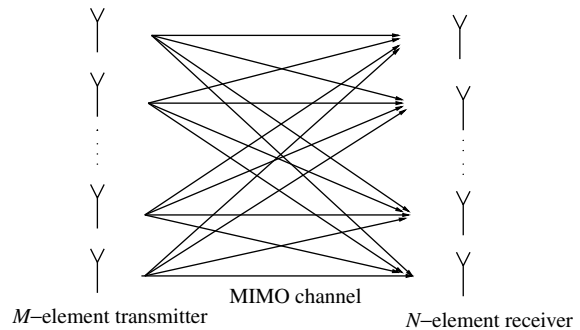


Fig. 1. Illustration of an MIMO system, the transmitter has  $M$  antenna elements and the receiver has  $N$  antenna elements.

## 2. MIMO Channel Modeling

### 2.1. Data Model

Figure 1 shows an MIMO system with  $M$  transmit elements and  $N$  receive elements. For the above MIMO propagation channel, the baseband input-output relationship can be expressed as

$$\mathbf{y}(t) = \mathbf{H}(t) * \mathbf{s}(t) + \mathbf{n}(t) \quad (1)$$

where  $\mathbf{s}(t)$  is the transmitted signal,  $\mathbf{y}(t)$  is the received signal,  $\mathbf{n}(t)$  is additive white Gaussian noise (AWGN) and  $*$  denotes convolution. Here  $\mathbf{H}(t)$  is an  $N$  by  $M$  channel impulse response matrix.

If the signal bandwidth is sufficiently narrow so that the channel can be treated as approximately constant over frequency (frequency flat channel), the corresponding input-output relationship simplifies to

$$\mathbf{y} = \mathbf{H}\mathbf{s} + \mathbf{n} \quad (2)$$

where  $\mathbf{H}$  is the narrowband MIMO channel matrix.

In many cases (e.g. Reference [1]), the elements of narrowband MIMO channel matrix are assumed to be independent and identically distributed (IID) to study the MIMO channel capacity. In reality, however, because of insufficient spacing between antenna elements and limited scattering in the environment, the fading is not always independent, causing a lower MIMO channel capacity compared to the ideal, IID case. Therefore, the proposed MIMO channel models should take this effect into account.

### 2.2. Model Classification

The modeling of the channel impulse response  $\mathbf{H}(t)$  (for the wideband system) or channel matrix  $\mathbf{H}$  (for

the narrowband system) is critical for the simulation of the MIMO communication systems and has attracted much interest recently. Several works have been reported in this area and the proposed models can be classified in different ways.

**Wideband Models vs. Narrowband Models.** The MIMO channel models can be divided into the wideband models and the narrowband models directly by considering the bandwidth of the system. The wideband models treat the propagation channel as frequency selective, which means that different frequency sub-bands have different channel responses. On the other hand, the narrowband models assume that the channel has frequency nonselective fading and therefore, the channel has the same response over the entire system bandwidth. Wideband MIMO channel models can be found in References [20–26] while References [27–34] treat narrowband models.

**Field Measurements vs. Scatterer Models.** To model the MIMO channel, one approach is to measure the MIMO channel responses through field measurements. Some important characteristics of the MIMO channel can be obtained by investigating the recorded data and the MIMO channel can be modeled to have similar characteristics. Models based on MIMO channel measurements were reported in References [20–23,29–31]. An alternative approach is to postulate a model (usually involving distributed scatterers) that attempts to capture the channel characteristics. Such a model can often illustrate the essential characteristics of the MIMO channel as long as the constructed scattering environment is reasonable. Examples of the scatterer models can be found in References [27,28].

**Nonphysical Models vs. Physical Models.** The MIMO channel models can be divided into the nonphysical and physical models. The nonphysical models are based on the channel statistical characteristics using nonphysical parameters. In general, the nonphysical models are easy to simulate and provide accurate channel characterization for the situations under which they were identified. On the other hand, they give limited insight to the propagation characteristics of the MIMO channels and depend on the measurement equipment, for example, the bandwidth, the configuration and aperture of the arrays, the heights and responses of transmit and receive antennas in the measurements. The influence of the channel and measurement equipment on the model cannot be

separated. Another category are the physical models. In general, these models choose some crucial physical parameters to describe the MIMO propagation channels. Some typical parameters include Angle of Arrival (AOA), Angle of Departure (AOD) and Time of Arrival (TOA). However, under many propagation conditions, the MIMO channels are not well described by a small number of physical parameters and this makes it difficult, if not impossible, to identify and validate the models. For instance, it was shown in Reference [35] that one might get a false AOA distribution through an artifact stemming from the measurement and identification procedure. Although one attempts to separate the propagation channel from the measurement equipment (antenna responses, configuration etc.) to allow extrapolation to other conditions, the model always contains some prejudice (e.g. point source assumptions) related to the conditions under which the model was identified. This always puts limitations on the model, which must be taken into account.

In this paper, we follow the last classification approach. The MIMO channel models are divided into two categories, that is, the nonphysical and physical modeling approaches. We will discuss these two groups of models in the following two sections respectively.

### 3. Non-physical MIMO Channel Models

#### 3.3. IST METRA Project

Under the European Union IST METRA (Multielement Transmit Receive Antennas) project, an indoor measurement campaign was carried out in Aalborg, Denmark at a carrier frequency of 2.05 GHz. A stochastic MIMO radio channel model for non-line-of-sight (NLOS) scenarios was proposed on the basis of the power correlation matrix of the MIMO radio channel [20,21].

Let  $M$  be the number of transmit antennas and  $N$  be the number of receive antennas. In the proposed wideband model, the MIMO channel without noise is expressed as

$$\mathbf{H}(\tau) = \sum_{l=1}^L \mathbf{H}_l \delta(\tau - \tau_l) \quad (3)$$

where  $\mathbf{H}(\tau)$  is the  $N \times M$  matrix of channel impulse responses and  $\mathbf{H}_l$  is the matrix of complex channel

coefficients at time delay  $\tau_l$ .

$$\mathbf{H}_l = \begin{bmatrix} H_{11}^l & H_{12}^l & \cdots & H_{1M}^l \\ H_{21}^l & H_{22}^l & \cdots & H_{2M}^l \\ \vdots & \vdots & \ddots & \vdots \\ H_{N1}^l & H_{N2}^l & \cdots & H_{NM}^l \end{bmatrix} \quad (4)$$

Moreover, the complex valued transmission coefficients are assumed to be zero-mean complex Gaussian and have the same average power  $p_l$ . The coefficients are independent from one time delay to another.

To construct the MIMO channel model, the correlation between different pairs of complex transmission coefficients need to be taken into account. The spatial correlation coefficients at the transmitter and receiver are considered in the proposed model,

$$\rho_{m_1 m_2}^{Tx} = \langle |H_{nm_1}^l|^2, |H_{nm_2}^l|^2 \rangle \quad (5)$$

$$\rho_{n_1 n_2}^{Rx} = \langle |H_{n_1 m}^l|^2, |H_{n_2 m}^l|^2 \rangle \quad (6)$$

where  $\rho_{m_1 m_2}^{Tx}$ ,  $\rho_{n_1 n_2}^{Rx}$  denote the power correlation coefficients at the transmitter and receiver, respectively. The correlation coefficient is defined as

$$\rho = \langle a, b \rangle = \frac{E[ab] - E[a]E[b]}{\sqrt{(E[a^2] - E[a]^2)(E[b^2] - E[b]^2)}} \quad (7)$$

where  $E[\cdot]$  denotes the expected value. Note that in this definition the spatial correlation on one side is assumed to be independent of the antenna elements on the opposite side.

It is claimed in Reference [21] that it can be shown theoretically [36] that the spatial cross correlation coefficient can be expressed as the product of the spatial correlation at the transmitter and receiver, that is,

$$\rho_{n_2 m_2}^{n_1 m_1} = \langle |H_{n_1 m_1}^l|^2, |H_{n_2 m_2}^l|^2 \rangle = \rho_{m_1 m_2}^{Tx} \rho_{n_1 n_2}^{Rx} \quad (8)$$

In matrix form, this can be written as

$$\mathbf{P}_H = \mathbf{P}_H^{Tx} \otimes \mathbf{P}_H^{Rx} \quad (9)$$

where ' $\otimes$ ' denotes the Kronecker product,  $\mathbf{P}_H$  is the power correlation matrix of the MIMO channel,  $\mathbf{P}_H^{Tx}$  and  $\mathbf{P}_H^{Rx}$  are the power correlation matrices seen from the transmitter and receiver, respectively.

Given the above spatial correlations, the MIMO radio channel can be easily simulated as

$$\text{vec}(\mathbf{H}_l) = \sqrt{p_l} \mathbf{C} \mathbf{a}_l \quad (10)$$

where  $\text{vec}(\cdot)$  denotes the vectorization operation (stacking the columns of the matrix into a vector) and  $\mathbf{a}_l$  is

a column vector with IID zero-mean complex Gaussian elements ( $MN$  by 1).  $\mathbf{C}$  is the symmetric mapping matrix and the  $(x, y)$ th element of  $\mathbf{C}\mathbf{C}^T$  equals the root of the power correlation coefficient between the  $x$ th and  $y$ th element of  $\mathbf{H}_l$ , where  $(\cdot)^T$  denotes transpose. The average power  $p_l$  can be decided by the power delay spectrum (PDS).

Narrowband MIMO channels, that is,  $L = 1$  were generated from the model and compared with measured data on the basis of the cumulative density function (CDF) of the eigenvalues. It was reported that the simulated channels agree well with the measurements.

One drawback of the above model is that the phase relationship between transmission coefficients is lost since the power correlation coefficients do not take the phase information into account. In Reference [21], it was suggested to multiply a phase steering diagonal matrix  $\mathbf{W}(\bar{\phi}_{Rx})$  after the convolution between the MIMO channel impulse response and the transmitted signal; therefore, the received signal without noise can be written as

$$\mathbf{y}(t) = \mathbf{W}(\bar{\phi}_{Rx}) \int \mathbf{H}(\tau) \mathbf{s}(t - \tau) d\tau \quad (11)$$

where the diagonal elements of the diagonal matrix  $\mathbf{W}(\bar{\phi}_{Rx})$  provide the average phase-shift information relative to the first receive element and  $\bar{\phi}_{Rx}$  is the mean azimuth AOA.

### 3.2. IST SATURN Project: Narrowband Model

In Bristol, an indoor measurement campaign was conducted under the EU IST SATURN (Smart Antenna Technology in Universal bRoadband wireless Networks) project [7]. On the basis of the first and second order moments of the measured data, a narrowband statistical model for NLOS MIMO propagation channels was presented in References [29,30].

It was found [29,30] that in the typical NLOS scenarios, the channel coefficients are zero-mean complex Gaussian. Furthermore, it was reported that the channel covariance matrix can be well approximated by the Kronecker product of the covariance matrices seen from both ends for such cases, that is,

$$\mathbf{R}_H = \mathbf{R}_H^{Tx} \otimes \mathbf{R}_H^{Rx} \quad (12)$$

where  $\mathbf{R}_H$  is the channel covariance matrix,  $\mathbf{R}_H^{Tx}$  and  $\mathbf{R}_H^{Rx}$  are the covariance matrices at the transmit and receive side, respectively.

$$\mathbf{R}_H^{Tx} = E[\mathbf{h}_i^H \mathbf{h}_i^T], \quad \text{for } i = 1, \dots, N \quad (13)$$

$$\mathbf{R}_H^{Rx} = E[\mathbf{h}^j \mathbf{h}^{jH}], \quad \text{for } j = 1, \dots, M \quad (14)$$

$$\mathbf{R}_H = E[\text{vec}(\mathbf{H})\text{vec}^H(\mathbf{H})] \quad (15)$$

where  $\mathbf{h}_i$  is the  $i$ th row of  $\mathbf{H}$ ,  $\mathbf{h}^j$  is the  $j$ th column of  $\mathbf{H}$  and  $(\cdot)^H$  is the complex conjugate transpose.

In Reference [37], the same structure was proposed in which the amplitude correlation was verified using the WiSE ray-tracing simulator. It is obvious that the expressions in (9) and (12) are related. In Equation (12), the channel covariance matrix is used instead of the power correlation matrix; therefore, Equation (12) provides the phase information of the MIMO propagation channel. The structure (12) was also discussed in the 3GPP (3rd Generation Partnership Project) meeting [38].

Assuming that the channel coefficients are zero-mean complex Gaussian, the first and second order moments of the MIMO channel are enough to characterize the propagation channel [39]. It is easy to show from Equation (12), as in Reference [26], that

$$\mathbf{H} = (\mathbf{R}_H^{Rx})^{1/2} \mathbf{G} (\mathbf{R}_H^{Tx})^{T/2} \quad (16)$$

where  $\mathbf{G}$  is a stochastic  $N$  by  $M$  matrix with IID  $\mathcal{CN}(0, 1)$  elements. Here,  $(\cdot)^{1/2}$  denotes any matrix square root such that  $\mathbf{R}^{1/2}(\mathbf{R}^{1/2})^H = \mathbf{R}$ . This model was first conjectured in Reference [40] to study the channel capacity. Notice that this model is also a special case of the model suggested in Reference [28]; we will revisit this shortly.

### 3.3. IST SATURN Project: Wideband Model

A wideband NLOS MIMO channel model was proposed in References [22,23] on the basis of the same sets of measured data. It was reported that for each tap, the normalized MIMO channel covariance matrix can be well modeled by the Kronecker product of the covariance matrices at both ends, that is,

$$\mathbf{R}_H^l = \mathbf{R}_{Tx}^l \otimes \mathbf{R}_{Rx}^l \quad (17)$$

where the channel covariance matrix of the  $l$ th tap of MIMO channel-impulse response  $\mathbf{R}_H^l$ , the covariance matrix of the  $l$ th tap seen from the transmit side  $\mathbf{R}_{Tx}^l$  and the covariance matrix of the  $l$ th tap seen from the receive side  $\mathbf{R}_{Rx}^l$  are defined similarly as in Equations (15), (13) and (14).

Assume that the taps are independent zero-mean complex Gaussian, the  $l$ th tap of the wideband MIMO channel impulse response can be modeled as

$$\mathbf{H}_l = (\mathbf{R}_{Rx}^l)^{1/2} \mathbf{G}_l (\mathbf{R}_{Tx}^l)^{T/2} \quad (18)$$

where  $\mathbf{H}_l$  is the  $l$ th tap of MIMO channel impulse response  $\mathbf{H}$  and  $\mathbf{G}_l$  is the matrix with IID zero-mean complex Gaussian elements of power  $\bar{p}_l$ . The power of the  $l$ th tap,  $\bar{p}_l$ , can be determined from the average power delay profile.

Finally, it should be noted that the elements of  $\mathbf{G}$  can be modeled by different SISO models [17,16,11]; therefore this wideband statistical model is flexible to different model requirements and scenarios. One example can be found in Reference [22] in which a tapped delay line SISO model [17] was combined with this wideband model.

## 4. Physical MIMO Channel Models

### 4.1. One-ring and Two-ring Models

In References [27,41], the narrowband ‘one-ring’ and ‘two-ring’ models were presented. Next, we will discuss these two models, respectively.

In the one-ring model, the base station (BS) is assumed to be elevated and therefore not obstructed by local scattering while the mobile station (MS) is surrounded by scatterers. No line-of-sight (LOS) is assumed between the BS and MS. Figure 2 illustrates this scenario in which  $T_p$  is the  $p$ th antenna element at the BS,  $R_n$  is the  $n$ th antenna element at the MS,  $D$  is the distance between the BS and MS,  $R$  is the radius of the ring of scatterers,  $\alpha$  is the AOA at the BS, and  $\gamma$  is the angle spread. Since  $D$  and  $R$  are much larger than the spacing between antenna elements,  $\gamma \approx \arcsin(R/D)$ . Denote the effective scatterer on the ring by  $S(\theta)$  and let  $\theta$  be the angle between the scatterer and the array at the MS. In the model, it is assumed that  $S(\theta)$  is uniformly distributed in  $\theta$  and the phase shift,  $\phi(\theta)$ , associated with each scatterer,  $S(\theta)$ , is distributed uniformly over  $[-\pi, \pi)$ . Each ray is further assumed to be reflected only once and all rays reach the receive array with the same power.

Suppose there are  $K$  effective scatterers  $S(\theta_k)$ ,  $k = 1, 2, \dots, K$  distributed on the ring, the complex

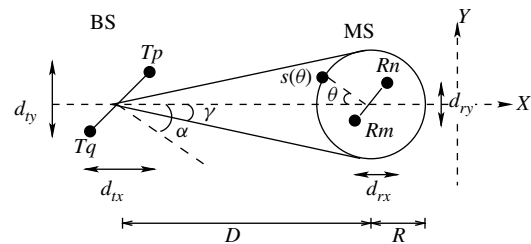


Fig. 2. Illustration of the one-ring model.

channel coefficient between the  $p$ th elements at the BS and  $n$ th element at the MS can be expressed as

$$H_{p,n} = \frac{1}{\sqrt{K}} \sum_{k=1}^K \exp \left\{ -j \frac{2\pi}{\lambda} (D_{T_p \rightarrow S(\theta_k)} + D_{S(\theta_k) \rightarrow R_n}) + j\phi(\theta_k) \right\} \quad (19)$$

where  $D_{X \rightarrow Y}$  denotes the distance between  $X$  and  $Y$  and  $\lambda$  is the wavelength. Because of the central limit theorem, when the number of scatterers becomes large, the channel coefficient is Gaussian distributed. The covariance between  $H_{p,n}$  and  $H_{q,m}$  is given by

$$E[H_{p,n} H_{q,m}^H] = \frac{1}{K} \sum_{k=1}^K \exp \left\{ -j \frac{2\pi}{\lambda} (D_{T_p \rightarrow S(\theta_k)} - D_{T_q \rightarrow S(\theta_k)} + D_{S(\theta_k) \rightarrow R_n} - D_{S(\theta_k) \rightarrow R_m}) \right\} \quad (20)$$

In general, Equation (20) has to be evaluated by numerical analysis. However, when the angle spread  $\gamma$  is small, some approximation can be made and it is possible to get some insights of the MIMO channel properties. The readers may refer to Reference [27] for more discussions about this issue.

The two-ring model assumes that both the BS and MS are surrounded by scatterers. This can be the case for indoor wireless communications. An illustration of the two-ring model is shown in Figure 3. Notice that in this model, each ray is reflected twice and the channel coefficient for the two-ring model is

$$H_{p,n} = \frac{1}{\sqrt{K_1 K_2}} \sum_{k=1}^{K_1} \sum_{l=1}^{K_2} \exp \left\{ -j \frac{2\pi}{\lambda} (D_{T_p \rightarrow S_1(\theta_k)} + D_{S_1(\theta_k) \rightarrow S_2(\theta_l)} + D_{S_2(\theta_l) \rightarrow R_n}) + j\phi_1(\alpha) + j\phi_2(\beta) \right\} \quad (21)$$

The difficulty in this model is that the signals reflected by the scatterers at the receive side are possibly not independent. Even if the numbers of scatterers,  $K_1$  and  $K_2$  go to infinity, the channel coefficient is still not zero-mean complex Gaussian. Therefore, the channel covariance matrix cannot completely

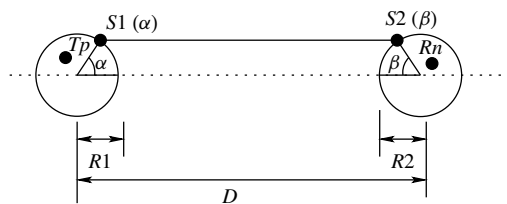


Fig. 3. Illustration of the two-ring model.

describe the MIMO channel. It was suggested in Reference [41] to generate the channel realizations using ray-tracing method (21) and to investigate the channel properties by Monte-Carlo simulations.

## 4.2. Von Mises Angular Distribution

Similar to the one-ring model, a narrowband model was proposed in References [32,33] that uses the von Mises angular probability density function (PDF) as the angular PDF at the mobile side and takes the Doppler spread into account. Figure 4 illustrates this model. Assume that the angle spread at the BS,  $\gamma$  is small and  $D \gg R \gg \max(d_{pq}, d_{nm})$  where  $d_{pq}$  and  $d_{nm}$  are the element spacing at the BS and MS, respectively; the cross covariance between two normalized channel coefficients can be approximated as follows: [32]

$$E[H_{p,n}(t) H_{q,m}^H(t + \tau)] = \int_0^{2\pi} \exp \left\{ \frac{j2\pi}{\lambda} [d_{pq}\gamma \sin(\alpha) \cdot \sin(\theta) + d_{nm} \cos(\theta - \beta)] - j2\pi f_D \times [\cos(\theta - \phi)]\tau \right\} p(\theta) d\theta \exp \left\{ \frac{j2\pi d_{pq} \cos(\alpha)}{\lambda} \right\} \quad (22)$$

where  $f_D = v/\lambda$  is the Doppler shift,  $v$  is the speed of the MS,  $\phi$  is the moving direction of the MS, and  $\tau$  is the relative time difference between the two links  $H_{p,n}$  and  $H_{q,m}$ . Note that this narrowband model includes information of temporal variations.

Compared with some previously measured data, it was reported in Reference [42] that the von Mises angular PDF is a good model for the angular PDF,  $p(\theta)$ . The von Mises PDF is defined by

$$p(\theta) = \frac{\exp[\kappa \cos(\theta - \mu)]}{2\pi I_0(\kappa)}, \quad \theta \in [-\pi, \pi] \quad (23)$$

where  $I_0(\cdot)$  is the zero order modified Bessel function and  $\mu$  is the mean AOA at the MS. The parameter  $\kappa$  can be chosen between 0 (isotropic scattering) and  $\infty$  (extreme nonisotropic scattering). Inserting the

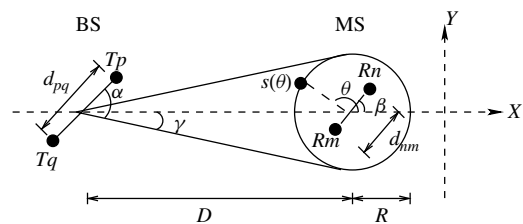


Fig. 4. Illustration of the model using von Mises angular distribution.

von Mises PDF to Equation (22) and calculating the integral [43], the covariance can be written as [32]

$$E[H_{p,n}(t)H_{q,m}^H(t+\tau)] = \frac{\exp[jc_{pq}\cos(\alpha)]}{I_o(\kappa)} I_0(\{\kappa^2 - a^2 - b_{nm}^2 - c_{pq}^2\gamma^2 \sin^2(\alpha) + 2ab_{nm}\cos(\beta - \phi) + 2c_{pq}\gamma \sin(\alpha)[a\sin(\phi) - b_{nm}\sin(\beta)] - j2\kappa \times [a\cos(\mu - \phi) - b_{nm}\cos(\mu - \beta) - c_{pq}\gamma \sin(\alpha) \times \sin(\mu)]\}^{1/2}) \quad (24)$$

where  $a = 2\pi f_D \tau$ ,  $b_{nm} = 2\pi d_{nm}/\lambda$  and  $c_{pq} = 2\pi d_{pq}/\lambda$ . Notice that this model was extended in Reference [33] to include the LOS component.

One important advantage of using the von Mises angular distribution is that it gives a closed-form expression and therefore, can be used to study the channel covariance analytically. As an example, a  $2 \times 2$  setup MIMO channel was studied [32] for the validation of the Kronecker structure in Equation (12). It was reported [32] that as the spacing of antenna elements increases, the normalized model error of the Kronecker structure does not decrease monotonically, which indicates the existence of local maxima. Furthermore, it was found that only for some specific antenna element spacings, the model error becomes zero and when the spacing is large, the model error is negligible.

### 4.3. Distributed Scattering Model

This narrowband model was proposed in Reference [28] to describe outdoor MIMO propagation channels. Figure 5 illustrates an NLOS outdoor propagation scenario. Assume there are  $M$  transmit elements and  $N$  receive elements. Both the transmitter and receiver are obstructed by the surrounding scatterers where the distance between the scatterers and transmitter/receiver is large enough so that the plane wave assumption holds.

Assume there are  $S$  scatterers on both the transmitter and receiver in which  $S$  is large enough to have random fading. The scatterers at the receive side can be seen as a virtual array between the transmitter and receiver. The MIMO channel transfer function is given by

$$\mathbf{H} = \frac{1}{\sqrt{S}} \mathbf{R}_{\theta_r, d_r}^{1/2} \mathbf{G}_r \mathbf{R}_{\theta_s, 2D_r/S}^{1/2} \mathbf{G}_t \mathbf{R}_{\theta_t, d_t}^{T/2} \quad (25)$$

where  $\frac{1}{\sqrt{S}}$  is a normalization factor,  $\mathbf{G}_t$  ( $S$  by  $M$ ) and  $\mathbf{G}_r$  ( $N$  by  $S$ ) are random matrices with IID zero-mean complex Gaussian elements.  $\mathbf{R}_{\theta_t, d_t}$ ,  $\mathbf{R}_{\theta_s, 2D_r/S}$ ,  $\mathbf{R}_{\theta_r, d_r}$  are the correlation matrices seen from the transmitter,

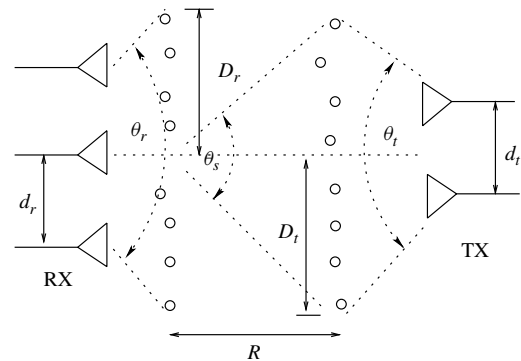


Fig. 5. Illustration of the distributed scattering model.

virtual array, and receiver, respectively. Notice that Equation (25) does not give Gaussian distribution unless  $\mathbf{R}_{\theta_r, 2D_r/S}$  has a high rank.

For uniformly distributed AOAs, the  $(m, k)$ th element of the correlation matrix can be expressed as [44–46]

$$[\mathbf{R}_{\theta,d}]_{m,k} = \frac{1}{S} \sum_{i=-\frac{S-1}{2}}^{\frac{S-1}{2}} e^{-2\pi j(k-m)d \cos\left(\frac{\pi}{2} + \theta_i\right)} \quad (26)$$

where  $S$  should be odd,  $d$  is the array element distance and  $\theta_i$  is the AOA of the  $i$ th scatterer. It is further assumed that the mean AOA is at the bore-sight of the array for the simplicity of the model. Note that other kinds of AOA distributions [46] can also be used but will lead to different expressions of the correlation matrix  $\mathbf{R}_{\theta,d}$ .

In general, when the angle spread of the AOA is small and/or the array interelement distance is small, the correlation matrix will lose rank. On the contrary, for large angle spread and/or large interelement distance, the correlation matrix will converge to the identity matrix, that is, a full rank matrix. Therefore, if the correlation matrix at the transmit and/or receive side is of low rank, then from Equation (26), the MIMO radio channel will be of low rank. The opposite, however, is not the case. Even if both the correlation matrices at the transmit and receive side are of high rank, the rank of channel matrix is still controlled by the correlation matrix of the virtual array,  $\mathbf{R}_{\theta_s, 2D_r/S}$ . The matrix  $\mathbf{R}_{\theta_s, 2D_r/S}$  is determined by the angle spread,  $\theta_s$ , and the spacing of the receive scatterers. The angle spread for the virtual array is defined by

$$\tan(\theta_s/2) = D_t/R \quad (27)$$

When the distance  $R$  is large compared with the product of  $D_t$ ,  $D_r$ , the virtual array correlation matrix will be of low rank and consequently the MIMO

channel will be of low rank. This effect is termed the ‘pinhole’ effect in Reference [28]. Note that the same effect was reported in Reference [47] but with the name the ‘keyhole’ effect. However, no observations of ‘pinhole’ effect from field measurements have been referenced or reported in the literature.

Consider extreme cases in the low-rank region where the correlation matrix  $\mathbf{R}_{\theta_s, 2D_r/S}$  is an all one matrix. In such a case, the channel matrix becomes rank one and the multiplexing gain is lost. On the other hand, in the high-rank region,  $\mathbf{R}_{\theta_s, 2D_r/S}$  converges to the identity matrix. Using the central limit theory, it is easy to show that when the number of scatterers at both sides is sufficiently large, the channel matrix approaches the model in Equation (16).

#### 4.4. Extended Saleh–Valenzuela Model

In Reference [11], a wideband SISO multipath channel model was proposed for the indoor scenario on the basis of the indoor measurements. The multipath components were observed to arrive in groups and therefore, the scatterers could be separated into clusters. Including the statistics of AOA and AOD, the Saleh–Valenzuela Model was extended to MIMO channels in Reference [31]. A narrowband MIMO channel model was then derived to compare with the measured data. Figure 6 shows the model parameters for a single cluster in the extended Saleh–Valenzuela model.

Suppose there are  $L$  clusters and each cluster has  $K$  rays, the directional channel response can be expressed as [31]

$$h(\theta^R, \theta^T) = \frac{1}{\sqrt{LK}} \sum_{l=0}^{L-1} \sum_{k=0}^{K-1} \beta_{kl} \delta(\theta^T - \Theta_l^T - \omega_{kl}^T) \times \delta(\theta^R - \Theta_l^R - \omega_{kl}^R) \quad (28)$$

where  $\theta^T$  and  $\theta^R$  are the transmit and receive angle,  $\beta_{kl}$  is the complex ray gain,  $\Theta_l^T$  and  $\Theta_l^R$  are the mean transmit and receive cluster arrival angles, and  $\omega_{kl}^T$  and  $\omega_{kl}^R$  are the relative transmit and receive angles for the  $k$ th ray in the  $l$ th cluster. On the basis of

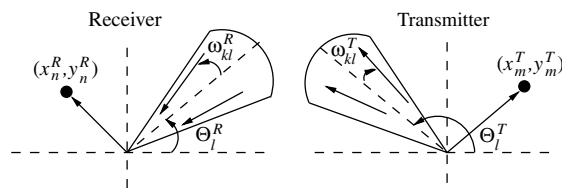


Fig. 6. Model parameters for a single cluster in the extended Saleh–Valenzuela model.

the measured data, it was proposed in Reference [48] to use a two-sided Laplacian distribution for the ray AOA/AOD, that is,

$$p(\omega) = \frac{1}{\sqrt{2}\sigma} \exp\left(-\left|\frac{\sqrt{2}\omega}{\sigma}\right|\right) \quad (29)$$

where  $\sigma$  is the angular standard deviation.

The rays in each cluster are assumed to be zero-mean complex Gaussian with power  $|\beta_l|^2$ . The cluster amplitude is Rayleigh distributed with  $E\{|\beta_l|^2\} = \exp(-T_l/\Gamma)$ , where  $\Gamma$  is the cluster decaying constant and  $T_l$  is the arrival time of the  $l$ th cluster [11,48]. On the basis of the above assumptions, the coefficient of the narrowband channel matrix is given by Reference [31]

$$H_{nm} = \int_{2\pi} \int_{2\pi} W_n^R(\theta^R) h(\theta^R, \theta^T) W_m^T(\theta^T) d\theta^T d\theta^R \quad (30)$$

where  $W_q^P(\theta) = G_q^P \exp[j\psi_q^P(\theta)]$ ,  $G_q^P$  is the antenna gain pattern,  $\psi_q^P(\theta) = 2\pi[x_q^P \cos(\theta) + y_q^P \sin(\theta)]$ ,  $P \in \{T, R\}$ , and  $q \in \{m, n\}$ .

A narrowband indoor MIMO channel measurement campaign was carried out and the data were collected from different measurement scenarios. All the scenarios showed rich scattering. The proposed model was compared with the models proposed in References [21,29,30] and better agreement with the measured data based on the channel capacity PDF, was reported. However, the reader should notice that since the data were collected from different scenarios, the power correlation matrix and channel covariance matrix might vary from one scenario to another. If this is not taken into account, the models in References [21,29,30] will, of course, be less accurate.

#### 4.5. COST 259 Directional Channel Model

A directional channel model developed by the European research initiative COST 259 was reported in Reference [25] and can be used to model different MIMO propagation channels. Suppose that the received impinging waves are plane and there are  $L$  impinging waves at the receiver. The double directional channel impulse response (DDCIR) can be expressed as [25]

$$h(\vec{r}, \tau, \theta^R, \theta^T) = \sum_{l=1}^{L(\vec{r})} h_l(\vec{r}, \tau, \theta^R, \theta^T) \quad (31)$$

where  $\vec{r}$  denotes the location of the receiver with respect to the transmitter,  $\tau$  is the time delay,  $\theta^R$  and  $\theta^T$  is the corresponding AOA and AOD at the receiver and transmitter, respectively.  $h_l(\vec{r}, \tau, \theta^R, \theta^T)$



is the channel response of the  $l$ th impinging wave. Notice that the clustering effect can be included [25] by some minor modification of Equation (31).

Given the positions of the  $m$ th transmit element and the  $n$ th receive element measured from any fixed reference point on the corresponding array, the DDCIR between these two elements is given by

$$H_{nm}(\vec{r}, \tau, \theta^R, \theta^T) = \sum_{l=1}^{L(\vec{r})} H_{nm}^l(\vec{r}, \tau, \theta^R, \theta^T) \quad (32)$$

where  $H_{nm}^l(\vec{r}, \tau, \theta^R, \theta^T)$  equals to  $h_l(\vec{r}, \tau, \theta^R, \theta^T)$  with a certain phase shift, which depends on the positions of both the transmit and receive elements.

Assume  $\vec{r} = \vec{r}(t)$ , which is time dependent and the scatterers are stationary, this will give a time-variant DDCIR,  $H_{nm}(t, \tau, \theta^R, \theta^T)$ . The nonangle resolved channel impulse response can then be derived as [25]

$$H_{nm}(t, \tau) = \int_{\theta^R} G_n^R(\theta^R) H_{nm}(t, \tau, \theta^R, \theta^T) d\theta^R \quad (33)$$

where  $G_n^R(\theta^R)$  is the complex antenna pattern for the  $n$ th receive element and

$$H_{nm}(t, \tau, \theta^R) = \int_{\theta^T} G_m^T(\theta^T) H_{nm}(t, \tau, \theta^R, \theta^T) d\theta^T \quad (34)$$

where  $G_m^T(\theta^T)$  is the complex antenna pattern for the  $m$ th transmit element.

To simulate the channel, a layered approach was proposed in Reference [25] where different environments have been separated into three levels. The top level is the cell type and each cell type includes a number of radio environments (second level). For each radio environment, some propagation scenarios (third level) have been identified. The parameters in the second level are referred to as Global Parameters (GPs), while those in the third level are called Local Parameters (LPs). In general, the propagation environment can be described by a number of external parameters, such as the frequency band, the height of BS and MS. The GPs are usually a set of PDFs and/or statistical moments characterizing the specific propagation environment. The parameters of the impinging waves are a possible set of LPs. The GPs are determined by the field measurements and decide the statistical properties of the LPs. See Reference [25] for more details about the model parameters and implementation aspects.

#### 4.6. EM Scattering Model

A physical MIMO model was presented in Reference [26] on the basis of Electromagnetic (EM) considerations. Both the properties of the channel and the

antennas were taken into account. In the uplink case, let the waves transmitted from the MS be reflected once by the surrounding effective scatterers (including some properties of multiple scattering) before reaching the BS, the channel impulse response for the link between the  $p$ th element at the MS and the  $n$ th element at the BS is given by

$$H_{p,n}(t, \tau) = \sum_{k=1}^K \frac{\sin c[\omega(\tau - \tau_k)]}{(|\vec{r}_{m_p s_k}| + |\vec{r}_{s_k b_n}|)} G_T(\vec{r}_{m_p s_k}) \times G_R(-\vec{r}_{s_k b_n}) \vec{g}_R(-\vec{r}_{s_k b_n}) \vec{S}_k \vec{g}_T(\vec{r}_{m_p s_k}) \quad (35)$$

where  $K$  is the number of scatterers,  $\omega$  is the system bandwidth, and  $\tau_k = (|\vec{r}_{m_p s_k}| + |\vec{r}_{s_k b_n}|)/c$ . Here,  $c$  is the speed of light in the surrounding medium. Let  $\vec{r}_{m_p s_k}$  be the vector from the mobile element  $p$  to the  $k$ th scatterer and let  $\vec{r}_{s_k b_n}$  be the vector from the  $k$ th scatterer to the  $n$ th element at the BS. The scattering dyad is denoted  $\vec{S}_k$  and contains the amplitude and direction information,  $G_T(\cdot)$  is the transmit antenna element pattern, and  $\vec{g}_T(\cdot)$  is the orientation of the transmitted field. Also, let  $G_R(\cdot)$  and  $\vec{g}_R(\cdot)$  be the same functions but at the receive side. Note that it is straightforward to extend this model to the downlink scenario.

For a narrowband MIMO system, the channel coefficient can be simply obtained by replacing the  $\sin c(\cdot)$  function in Equation (35) with a phase shift,  $e^{-j\omega_c \tau_k}$ , where  $\omega_c$  is the carrier frequency of the system.

This model includes the antenna polarization properties through the antenna functions. It is a function of time and thus reflects the time evolution of the MIMO channel. Therefore, the Doppler shift is implicitly included in this model. One disadvantage might be to derive the scattering dyad  $\vec{S}_k$ , since one must consider the properties of the effective scattering objects that include the effects of multiple reflections and this will influence the accuracy and complexity of the model. Note that if the scatterers are too close to the BS or MS, the near field effect should also be considered.

#### 4.7. Virtual Channel Model

Suppose there are  $K$  scatterers (within one cluster) between the transmitter and receiver, one physical MIMO channel model for this cluster is [24]

$$\mathbf{H} = \sum_{k=1}^K \beta_k \mathbf{a}_R(\phi_{R,k}) \mathbf{a}_T^H(\phi_{T,k}) \quad (36)$$

where  $\beta_k$  is the path gain for the  $k$ th scatterer. Let  $\phi_{T,k}$  and  $\phi_{R,k}$  be the AOD and AOA, respectively. Assume

both the transmit and receive arrays are uniform linear arrays (ULAs), the impinging waves are plane. The array response vectors at both sides are given by

$$\mathbf{a}_T(\phi_{T,k}) = [1, e^{-j2\pi\theta_{T,k}}, \dots, e^{-j2\pi(M-1)\theta_{T,k}}]^T \quad (37)$$

$$\mathbf{a}_R(\phi_{R,k}) = [1, e^{-j2\pi\theta_{R,k}}, \dots, e^{-j2\pi(N-1)\theta_{R,k}}]^T \quad (38)$$

where  $\theta_{T,k} = d_t \sin(\phi_{T,k})/\lambda$ , and  $\theta_{R,k} = d_r \sin(\phi_{R,k})/\lambda$ . The wavelength is  $\lambda$ , and  $d_t$  and  $d_r$  are the element spacings of the transmit and receive array, respectively. In matrix form, Equation (36) can be written as

$$\mathbf{H} = \mathbf{A}_R \mathbf{H}_P \mathbf{A}_T^H \quad (39)$$

where  $\mathbf{A}_T = [\mathbf{a}_T(\phi_{T,1}), \dots, \mathbf{a}_T(\phi_{T,K})]$  is a  $M$  by  $K$  matrix,  $\mathbf{A}_R = [\mathbf{a}_R(\phi_{R,1}), \dots, \mathbf{a}_R(\phi_{R,K})]$  is a  $N$  by  $K$  matrix and the  $K \times K$  diagonal matrix  $\mathbf{H}_P = \text{diag}(\beta_1, \dots, \beta_K)$ . This model, however, is nonlinear in  $\phi_{T,k}$  and  $\phi_{R,k}$ .

On the basis of the limited spatial resolution of the transmit and receive array, a linear model called virtual channel model was presented in Reference [34]. In the model, the virtual AOD,  $\psi_{T,p}$  and virtual AOA,  $\psi_{R,q}$  from different scatterers are fixed according to the number of elements at both sides, that is,

$$\psi_{T,p} = \sin^{-1} \left( \frac{a_p \lambda}{M d_t} \right), \quad \psi_{R,q} = \sin^{-1} \left( \frac{b_q \lambda}{N d_r} \right) \quad (40)$$

where  $a_i = -(M-1)/2, \dots, (M-1)/2$  when  $M$  is odd and  $a_i = -M/2, \dots, M/2$  when  $M$  is even.  $b_i = -(N-1)/2, \dots, (N-1)/2$  when  $N$  is odd and  $b_i = -N/2, \dots, N/2$  when  $N$  is even.

The MIMO channel matrix can be modeled as

$$\begin{aligned} \mathbf{H} &= \sum_{q=1}^N \sum_{p=1}^M \mathbf{H}_V(p, q) \mathbf{a}_R(\psi_{R,q}) \mathbf{a}_T^H(\psi_{T,p}) \\ &= \tilde{\mathbf{A}}_R \mathbf{H}_V \tilde{\mathbf{A}}_T^H \end{aligned} \quad (41)$$

where  $\mathbf{H}_V$  is the virtual channel representation,  $\tilde{\mathbf{A}}_T$  and  $\tilde{\mathbf{A}}_R$  are defined similarly as in Equation (39). Note that both  $\tilde{\mathbf{A}}_T$ ,  $\tilde{\mathbf{A}}_R$  are unitary matrices and  $\mathbf{H}_V$  is no longer a diagonal matrix in general.

This model is similar in spirit to the beamspace method used in array signal processing. For the MIMO channel with  $L$  distinct clusters, the channel can be separated into  $L$  parallel virtual channels [34], that is,  $\mathbf{H}_V(i)$ ,  $i = 1, \dots, L$ . The rank of the channel matrix  $\mathbf{H}$  is bounded by the sum of the ranks of the virtual channel matrices  $\mathbf{H}_V(i)$  and the channel capacity is the superposition of the capacity for each virtual channel.

## 5. Measurement Results

In this section, we present some indoor MIMO channel measurement results from the IST SATURN project and compare these results with some proposed models. More details about the measurements and data-processing procedures can be found in References [23,29,30].

The measurements were carried out using the Medav RUSK BRI vector sounder, which has an eight-element omnidirectional ULA at the transmit side and an eight-element ULA with  $120^\circ$  beamwidth at the receive side (for pictures, see Reference [7]). The distance between the neighboring elements was  $0.5\lambda$ . Coherence between the transmitter and receiver was maintained by a cable connection.

The measurements were centered at 5.2 GHz with 120 MHz bandwidth. The whole bandwidth was divided into 97 narrowband frequency subchannels and a periodic multifrequency signal was sent over the entire bandwidth. The channel response was estimated and recorded in the frequency domain at the receive side. Although both the LOS and NLOS scenarios were measured, only the results from the typical NLOS scenarios are considered, where the transmitter was located at five different positions (Tx11-Tx15) in a computer room while the receiver (Rx3) was located at the corner of another large modern office with cubicles. Although people were moving around in the vicinity of the measurement equipment, the measured MIMO channel was still quite static over the whole measurement time (5.3 s). By treating pairs of neighboring antenna elements and/or different frequency subchannels (if possible) as different channel realizations, the statistical characteristics of the NLOS MIMO indoor channels were studied. In the following section, we use the transmitter location Tx13 as an example; similar results are found for the other four transmitter locations.

### 5.1. Narrowband MIMO Channel

Figures 7 and 8 show the histogram of the envelope of MIMO channel coefficient and the CDF of the phase of MIMO channel coefficient, respectively. It is observed that the envelope is well described by a Rayleigh distribution and the phase by a uniform distribution over  $[-\pi/2, \pi/2]$ . Therefore, the channel coefficient is modeled by a zero-mean complex Gaussian random variable in these NLOS scenarios. For nonphysical models, this result means that the assumption about complex Gaussian channels is valid. While for physical models, the one-ring

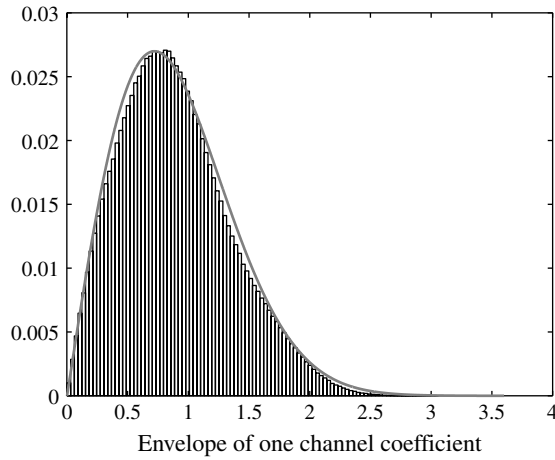


Fig. 7. Histogram of the envelope of one channel coefficient for NLOS indoor MIMO scenario (Tx13-Rx3) and the fitted Rayleigh distribution envelope (normalized).

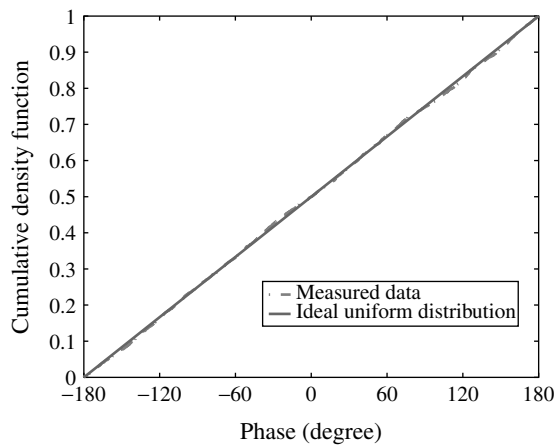


Fig. 8. CDF of the phase of one channel coefficient and the CDF of the uniform distribution within  $[-180^\circ, 180^\circ]$  (Tx13-Rx3).

model (each ray is reflected only once) is reasonable for the indoor scenarios. However, the two-ring model (reflected by the scatterers twice) appears to be unsuitable for such scenarios.

The Kronecker structure (12) of the normalized channel covariance matrix is investigated and compared with the results of an optimal Kronecker factorization [30]. It is shown in Table 1 that the approximation (12) is quite accurate and it is very close to the optimal factorization of the channel covariance matrix. In Table 1,  $\mathbf{X}$  and  $\mathbf{Y}$  are the positive definite Hermitian matrices resulting from the Kronecker factorization of the channel covariance matrix,  $\hat{(\cdot)}$  denotes sample covariance matrix, and the model

error  $\Psi$  is defined as

$$\Psi(\mathbf{A}, \mathbf{B}) = \frac{\|\mathbf{A} - \mathbf{B}\|_F}{\|\mathbf{A}\|_F} \quad (42)$$

where  $\|\cdot\|_F$  is the Frobenius norm.

To further verify the model in Equation (16), the channel matrix  $\mathbf{H}$  is then simulated according to Equation (16) and the corresponding channel capacity is compared with the measured data based on the CDF curve. The results are shown in Figure 9. As a reference, the capacity for the IID channel is also included in the same figure. It is shown that this narrowband statistical model tracks the measured results quite well. The measured data agrees with the model (16), which is also a special case of the distributed scattering model (25). However, the ‘pinhole’ effect was not observed from the measurement results.

## 5.2. Wideband MIMO Channel

The same sets of data as mentioned above are used and the MIMO channel impulse responses are obtained by using inverse Fourier transform with Hanning windowing. Each channel has 20 MHz bandwidth and therefore there are six parallel MIMO

Table I. List of Model Errors (Tx13-Rx3).

	$2 \times 2$	$3 \times 3$
$\Psi(\hat{\mathbf{R}}_H, \mathbf{X} \otimes \mathbf{Y})$	0.76%	4.52%
$\Psi(\hat{\mathbf{R}}_H, \hat{\mathbf{R}}_H^{Tx} \otimes \hat{\mathbf{R}}_H^{Rx})$	0.86%	4.79%
$\Psi(\hat{\mathbf{R}}_H^{Tx}, \mathbf{X})$	0.40%	1.74%
$\Psi(\hat{\mathbf{R}}_H^{Rx}, \mathbf{Y})$	0.03%	1.60%

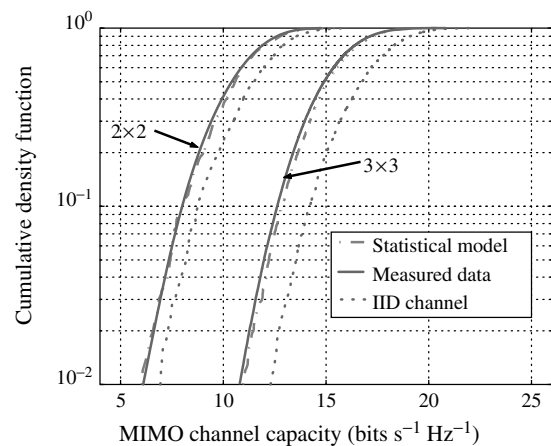


Fig. 9. Cumulative density function of channel capacity (Tx13-Rx3) for measured data, statistical model and IID MIMO channel. The signal-to-noise ratio (SNR) at the receive side is 20 dB. The power is equally allocated to the transmit elements.

channels for the whole 120 MHz measurement bandwidth. These six parallel MIMO channels are treated as different channel realizations to increase the number of MIMO channel impulse responses. The model errors of the Kronecker structure for each tap (17) are calculated and compared with the optimal Kronecker factorization. Figure 10 shows the model errors for the  $3 \times 3$  setup. Note that only those taps with significant power are displayed. It can be seen from the figure that the average model error for the  $3 \times 3$  case is below 10% (for  $2 \times 2$  case, the average model error is below 5%) and therefore the covariance matrix of each tap of the MIMO channel can be approximately modeled by the Kronecker structure. Furthermore, it is observed that the channel covariance matrices for those taps with significant power have relatively stable amplitudes while the phases are quite different. This phenomenon, however, still needs to be studied further.

The MIMO channel impulse responses are generated according to the model in Equation (18) and Fourier transform is used to transform the simulated impulse responses back into the frequency domain and the capacity of the narrowband MIMO channel is compared with that from the measured data (averaged in frequency domain for both cases and also over spatial domain for the measured data), see Figure 11. In both cases, there is reasonably good agreement between the measured data and the proposed wideband model (18).

## 6. Conclusions and Future Work

In this paper, we review some published works concerning MIMO channel modeling. Models are divided

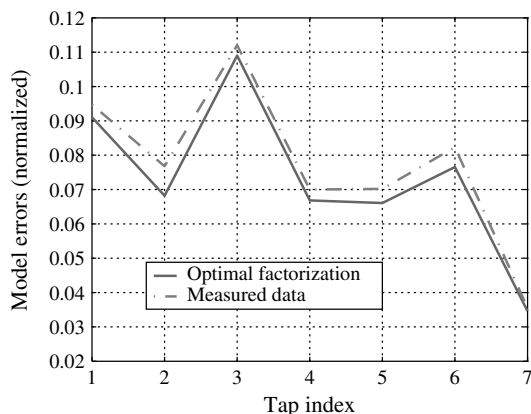


Fig. 10. Model errors of the Kronecker structure (normalized). The data set used is Tx13-Rx3 and the bandwidth of the channel impulse response is 20 MHz.

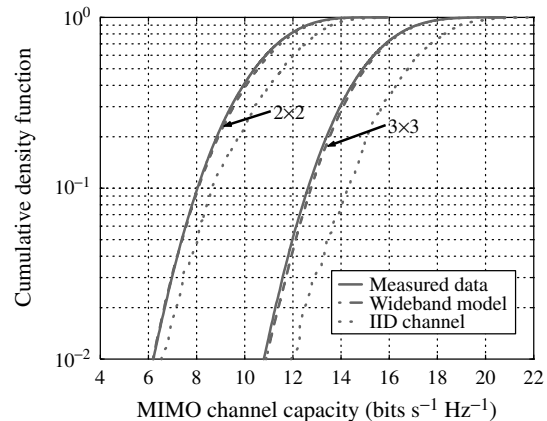


Fig. 11. CDF of narrowband channel capacity (normalized) for measured data (Tx13-Rx3), wideband model and IID MIMO channel. The power is equally allocated to the transmit elements, the SNR at the receive side is 20 dB.

into nonphysical and physical approaches. In the paper, the nonphysical models are all based on indoor MIMO channel measurements. Multiplicative structures of either the channel covariance matrix or the power correlation matrix are exploited to model the MIMO channel. Most of the physical models, on the other hand, postulate a scattering environment and derive an MIMO channel model involving scattering parameters. Still, an accurate description of the cross correlation between pairs of channel coefficients is one of the important modeling aims. In References [25,31], two parametric physical models were proposed in which the characteristics of the parameters are based on the results of the previous field measurements. The relationships between these different models are discussed in the paper.

Further research is required in this area. The following issues deserve more thorough investigation:

1. Initial simulations by the authors show that the one-ring model does not obey the Kronecker structure as shown in Equation (12). Model errors are large when both the BS and MS have high covariances between neighboring antenna elements. Similar simulation results are reported in Reference [49] using EM scattering model to simulate both microcell and indoor environments. The two-ring model has this structure, however, the channel coefficients are not random Gaussian variables. Therefore, theoretical analysis of the nonphysical models and validation of the physical models from measurements are required to bridge the gap between these two groups of models. A validated physical model can greatly reduce the number of

required measurements on designing MIMO communication systems and thus decrease the R&D costs.

2. Most published MIMO channel models assume NLOS scenarios. However, in some circumstances, the LOS exists and therefore models that describe LOS MIMO channels are also necessary. One nature approach is to separate the LOS component from the NLOS components and model them separately, for example, by mixing physical and non-physical model parameters. There are, of course, other methods to model the LOS channels.
3. Uptil now, no outdoor MIMO channel models have been reported on the basis of the MIMO channel measurements. The outdoor scenarios are very different from the indoor scenarios. For instance, in the indoor scenarios, the Doppler shift is small, while the outdoor scenarios may have relatively large Doppler shift. Therefore, to compare and validate those models for the outdoor MIMO propagation channels, the models based on outdoor MIMO channel measurements are necessary.

## Acknowledgement

The authors would like to thank Dr. Mats Bengtsson for useful discussions and suggestions.

## References

1. Foschini GJ, Gans MJ. On limits of wireless communications in a fading environment. *Wireless Personal Communications* 1998; **6**: 311–335.
2. Telatar IE. Capacity of multi-antenna Gaussian channels. *European Transactions on Telecommunications* 1999; **10**(6): 585–595.
3. Foschini GJ. Layered space-time architecture for wireless communication in a fading environment when using multiple antennas. *Bell Laboratories Technical Journal* 1996; **1**(2): 41–59.
4. Stridh R, Karlsson P, Ottersten B. MIMO channel capacity on a measured indoor radio channel at 5.8 GHz. In *Proceedings of the Asilomar Conference on Signals, Systems and Computers*, October 2000.
5. Martin CC, Winters JH, Sollenberger NR. Multiple-input-multiple-Output (MIMO) radio channel measurements. In *Proceedings of the IEEE Vehicular Technology Conference*, IEEE VTC Fall, 2000; pp. 774–779.
6. Kermoal JP, Mogensen PE, Jensen SH, Andersen JB. Experimental investigation of multipath richness for multi-element transmit and receive antenna arrays. In *Proceedings of the IEEE Vehicular Technology Conference*, IEEE VTC Spring, 2000; pp. 2004–2008.
7. McNamara DP, Beach MA, Fletcher PN, Karlsson P. Initial investigation of multiple-input multiple-output channels in indoor environments. In *Proceedings of the IEEE Benelux Chapter Symposium on Communications and Vehicular Technology*, Leuven, Belgium, October 2000.
8. Wallace JW, Jensen MA. Spatial characteristics of the MIMO wireless channel: experimental data acquisition and analysis. In *Proceedings of the IEEE International Conference on Acoustics, Speech and Signal Processing*, Vol. 4: 2001; pp. 2497–2500.
9. Molisch AF, Steinbauer M, Toeltsch M, Bonek E, Thoma RS. Capacity of MIMO systems based on measured wireless channels. *IEEE Journal on Selected Area in Communications* 2002; **20**(3): 539–549.
10. Kyrtsi P, Cox DC. Propagation characteristics of horizontally and vertically polarized electric fields in an indoor environment: simple model and results. In *Proceedings of the IEEE Vehicular Technology Conference*, IEEE VTC Fall, Vol. 3: 2001; pp. 1422–1426.
11. Saleh A, Valenzuela R. A statistical model for indoor multipath propagation. *IEEE Journal on Selected Areas in Communications* 1987; **SAC-5**(2): 128–137.
12. Rapoport TS, Seidel SY, Takamizawa K. Statistical channel impulse response models for factory and open plan building radio communication system design. *IEEE Transactions on Communications* 1991; **39**(5): 794–807.
13. Hashemi H. Impulse response modeling of indoor radio propagation channels. *IEEE Journal on Selected Areas in Communications* 1993; **11**(7): 967–978.
14. Howard SJ, Pahlavan K. Autoregressive modeling of wide-band indoor radio propagation. *IEEE Transactions on Communications* 1992; **40**(9): 1540–1552.
15. Ganesh R, Pahlavan K. Statistical modelling and computer simulation of indoor radio channel. *IEE Proceedings-I* 1991; **138**(3): 153–161.
16. Pahlavan K, Levesque AH. *Wireless Information Networks*. John Wiley & Sons, New York, 1995.
17. Medbo J, Andersson H, Schramm P, Asplund H, Berg JE. Channel Models for HIPERLAN/2 in Different Indoor Scenarios. COST 259 TD(98)70, April 1998.
18. Suzuki H. A statistical model for urban radio propagation. *IEEE Transactions on Communications* 1977; **COM-25**(7): 673–680.
19. Iwai H, Karasawa Y. Wideband propagation model for the analysis of the effect of the multipath fading on the near-far problem in CDMA mobile radio systems. *IEICE Transactions on Communications* 1993; **E76-B**(2): 103–112.
20. Kermoal JP, Schumacher L, Mogensen PE, Pedersen KI. Experimental investigation of correlation properties of MIMO radio channels for indoor picocell scenarios. In *Proceedings of the IEEE Vehicular Technology Conference*, IEEE VTC Fall, 2000; pp. 14–21.
21. Pedersen KI, Andersen JB, Kermoal JP, Mogensen P. A stochastic multiple-input-multiple-output radio channel model for evaluation of space-time coding algorithms. In *Proceedings of the IEEE Vehicular Technology Conference*, Fall, 2000; pp. 893–897.
22. Yu K, Bengtsson M, Ottersten B, McNamara D, Karlsson P, Beach M. A wideband statistical model for NLOS indoor MIMO channels. In *Proceedings of the IEEE Vehicular Technology Conference*, IEEE VTC Spring, Vol. 1: 2002; pp. 370–374.
23. Yu K, Bengtsson M, Ottersten B, McNamara D, Karlsson P, Beach M. A 20 MHz HiperLAN/2 MIMO channel model in NLOS indoor scenarios. In *Proceedings Konferensen RadioVetenskap och Kommunikation (RVK) '02*, 2002; pp. 311–315.
24. Stege M, Jelitto J, Brozel M, Fettweis G. A multiple input-multiple output channel model for simulation of Tx- and Rx-diversity wireless systems. In *Proceedings of the IEEE Vehicular Technology Conference*, IEEE VTC Fall, Vol. 2: 2000; pp. 833–839.
25. Correia LM (ed.). *Wireless Flexible Personalised Communications*. Chapter 3, John Wiley & Sons, 2001; pp. 77–277.
26. Svantesson T. A physical MIMO radio channel model for multi-element multi-polarized antenna systems. In *Proceedings*

- of the *IEEE Vehicular Technology Conference*, IEEE VTC Fall, Vol. 2: 2001; pp. 1083–1087.
27. Shiu D-S, Foschini GJ, Gans MJ, Kahn JM. Fading correlation and its effect on the capacity of multielement antenna systems. *IEEE Transactions on Communications* 2000; **48**(3): 502–513.
  28. Gesbert D, Bölcskei H, Gore D, Paulraj A, MIMO wireless channels: capacity and performance. In *Proceedings Global Telecommunications Conference*, Vol. 2, November 2000, pp. 1083–1088.
  29. Yu K, Bengtsson M, Ottersten B, Karlsson P, McNamara D, Beach M. Measurement analysis of NLOS indoor MIMO channels. In *Proceedings IST Mobile Communications Summit*, Barcelona, Spain, September 2001; pp. 277–282.
  30. Yu K, Bengtsson M, Ottersten B, McNamara D, Karlsson P, Beach M. Second order statistics of NLOS indoor MIMO channels based on 5.2 GHz measurements. In *Proceedings IEEE Globecom* 2001; Vol. 1, San Antonio, TX, November 2001, pp. 156–160.
  31. Wallace JW, Jensen MA. Statistical characteristics of measured MIMO wireless channel data and comparison to conventional models. In *Proceedings IEEE Vehicular Technology Conference*, IEEE VTC Fall, Vol. 2, 2001; pp. 1078–1082.
  32. Abdi A, Kaveh M. Space-time correlation modeling of multielement antenna systems in mobile fading channels. In *Proceedings International Conference on Acoustics, Speech, and Signal Processing*, May 2001.
  33. Abdi A, Kaveh M. A space-time correlation model for multielement antenna systems in mobile fading channels. *IEEE Journal on Selected Areas in Communications* 2002; **20**(3): 550–560.
  34. Sayeed A. Modeling and capacity of realistic spatial MIMO channels. In *Proceedings of IEEE International Conference on Acoustics, Speech, and Signal Processing*, Vol. 4, 2001; pp. 2489–2492.
  35. Bengtsson M, Völcger B. On the estimation of azimuth distributions and azimuth spectra. In *Proceedings IEEE Vehicular Technology Conference*. IEEE VTC Fall, October 2001; pp. 1612–1615.
  36. Eggers PCF, Toftgård J, Oprea AM. Antenna systems for base station diversity in urban small and micro cells. *IEEE Journal on Selected Areas in Communications* 1993; **11**(7): 1046–1057.
  37. Chuah C-N, Tse DNC, Kahn JM, and Valenzuela RA. Capacity scaling in MIMO wireless systems under correlated fading. *IEEE Transaction on Information Theory* 2002; **48**(3): 637–650.
  38. Lucent, Nokia, Siemens, Ericsson. A Standardized Set of MIMO Radio Propagation Channels. 3GPP, TSG RAN WG1, R1-01-1179, Jeju, Korea, November 2001.
  39. Kay SM. *Statistical Signal Processing: Estimation Theory*. Prentice Hall PTR: Upper Saddle River, NJ, 1993.
  40. Chizhik D, Rashid-Farrokhi F, Ling J, Lozano A. Effect of antenna separation on the capacity of BLAST of correlated channels. *IEEE Communications Letters* 2000; **4**(11): 337–339.
  41. Shiu D-S, Wireless Communication Using Dual Antenna Arrays. ISBN 0-7923-8680-9, Kluwer Academic Publishers: Norwell, MA, 2000.
  42. Abdi A, Kaveh M. A versatile spatio-temporal correlation function for mobile fading channels with non-isotropic scattering. In *Proceedings IEEE Workshop on Statistical Signal Array Processing*, 2000; pp. 58–62.
  43. Gradshteyn IS, Ryzhik IM. *Table of Integrals, Series, and Products*. 5th edition, Academic Press: New York, 1994.
  44. Astely D. On Antenna Arrays in Mobile Communication Systems: Fast Fading and GSM Base station Algorithms. Tech. Rep. IR-S3-SB-9611, Royal Institute of Technology, Stockholm, March 1996.
  45. Trump T, Ottersten B. Estimation of nominal direction of arrival and angular spread using an array of sensors. *Signal Processing* 1996; **50**(1-2): 57–69.
  46. Ertel RB, Cardieri P, Sowerby KW, Rappaport TS, Reed JH. Overview of spatial channel models for antenna array communication systems. *IEEE Personal Communications* 1998; **5**(1): 10–22.
  47. Chizhik D, Foschini GJ, Valenzuela RA. Capacities of multi-element transmit and receive antennas: correlation and keyholes. *Electronic Letters* 2000; **36**(13): 1099–1100.
  48. Spencer Q, Jeffs B, Jensen M, Swindlehurst L. Modeling the statistical time and angle of arrival characteristics of an indoor multipath channel. *IEEE Journal on Selected Areas in Communications* 2000; **18**(3): 347–360.
  49. Svantesson T. Antennas and Propagation from a Signal Processing Perspective. Ph.D. thesis, Chalmers University of Technology, Sweden, 2001.

## Authors' Biographies



**Kai Yu** was born on 18 September 1976 in Shanghai, China. He received his B.Eng. degree from Shanghai University in 1998 and M.Sc. degree (with Distinction) from the University of Liverpool, UK in 2000, respectively. Both degrees are in Electrical Engineering. He joined the Signal Processing Group, Royal Institute of Technology as a Ph.D. student in October 2000. His current research interests include multiple access techniques and MIMO channel modeling. Kai Yu is a student member of IEEE.



**Björn Ottersten** was born in Stockholm, Sweden, 1961. He received the M.S. degree in electrical engineering and applied physics from Linköping University, Linköping, Sweden, in 1986. In 1989, he received the Ph.D. degree in electrical engineering from Stanford University, Stanford, CA.

Dr. Ottersten has held research positions at the Department of Electrical Engineering, Linköping University, the Royal Institute of Technology, Stockholm, the Information Systems Laboratory, Stanford University, and the Department of Electrical Engineering, Katholieke Universiteit Leuven. Between the years 1996 and 1997, Dr. Ottersten was Director of Research at ArrayComm Inc, California. He has coauthored papers that received the Signal Processing Society Paper Award in 1993 and 2001.

In 1991, he was appointed Professor of Signal Processing at the Royal Institute of Technology (KTH), Stockholm, and he is currently head of the Department of Signals, Sensors & Systems at KTH. Dr. Ottersten is also a visiting professor at the Katholieke Universiteit Leuven, Leuven.

Dr. Ottersten is an associate editor for the *IEEE Transactions on Signal Processing*. His research interests include wireless communications, stochastic signal processing, sensor array processing, and time series analysis.